

Pseudo-Data based Self-Supervised Federated Learning for Classification of Histopathological Images

Jun Shi, *Member, IEEE*, Yuanming Zhang, Zheng Li, Xiangmin Han, Saisai Ding, Jun Wang, *Member, IEEE*, Shihui Ying, *Member, IEEE*

Abstract—Computer-aided diagnosis (CAD) can help pathologists improve diagnostic accuracy together with consistency and repeatability for cancers. However, the CAD models trained with the histopathological images only from a single center (hospital) generally suffer from the generalization problem due to the straining inconsistencies among different centers. In this work, we propose a pseudo-data based self-supervised federated learning (FL) framework, named SSL-FT-BT, to improve both the diagnostic accuracy and generalization of CAD models. Specifically, the pseudo histopathological images are generated from each center, which contains inherent and specific properties corresponding to the real images in this center, but does not include the privacy information. These pseudo images are then shared in the central server for self-supervised learning (SSL). A multi-task SSL is then designed to fully learn both the center-specific information and common inherent representation according to the data characteristics. Moreover, a novel Barlow Twins based FL (FL-BT) algorithm is proposed to improve the local training for the CAD model in each center by conducting contrastive learning, which benefits the optimization of the global model in the FL procedure. The experimental results on three public histopathological image datasets indicate the effectiveness of the proposed SSL-FL-BT on both diagnostic accuracy and generalization.

Index Terms—Histopathological image, federated learning, multi-center learning, self-supervised learning, Barlow twins contrastive learning

I. INTRODUCTION

Cancers seriously threaten human health. Histopathological diagnosis is the “gold standard” for the diagnosis of cancers in clinical practice [1]. However, it generally suffers from the issues of low efficiency, consistency and repeatability [2]. To this end, computer-aided diagnosis (CAD) for histopathological images has attracted considerable attention in recent years [3][4]. As a classical deep learning method, convolutional neural network (CNN) and its variants have proved their effectiveness as the backbone for the CAD models of histopathological images [3][4][5][6][7][8].

It is worth noting that even the most common and accessible type of stain, such as hematoxylin and eosin (H&E), will still produce different color intensities depending on the brand,

storage time, and temperature [1]. It then results in inconsistencies in the stained histopathological images among different hospitals. If the training samples are only acquired from one hospital, the generalization of a CAD model then will be degraded. To this end, a potential solution is to train the CAD model with the histopathological images from multiple hospitals (*i.e.*, multi-centers). Some pioneering works have indicated the feasibility and effectiveness of multi-center learning for improving the generalization of CNN models [9]. Moreover, this manner also can alleviate the problem of small sample size (SSS), which is a common issue in the field of CAD [4].

For multi-center learning, it is a common way to gather data from all centers together to train a model [10][11]. However, this training strategy suffers from the issues of privacy protection, data security and data ownership [12]. Federated learning (FL) then emerges as a promising solution, which can jointly train the CAD models by sharing parameters of distributed local models instead of the local data in the conventional multi-center learning paradigm [13][14]. This new multi-center learning paradigm has gained considerable attention in the field of healthcare [12][15], and it has been successfully applied for the CAD tasks [16][17], including for histopathological images [18]. However, it still cannot guarantee that the distributed CAD models fully capture the specific properties of different centers’ data, because FL only shares the model parameters instead of data, and the distributed local models do not contain enough specific information.

In recent years, image synthesis has achieved remarkable performances due to the fast development of generative adversarial network (GAN) and its variants [19][20][21]. The synthesized images generally have the characteristics of high resolution and high fidelity, which benefits the optimization of machine learning models. Thus, if some pseudo histopathological images are generated in each center, they can contain inherent and specific properties corresponding to the real histopathological images of the center, but do not include the privacy information. Thus, it is a feasible way to share these pseudo data to pre-train the backbone of CNN model in the central server, and then further conduct FL. This strategy can

This work is supported by National Natural Science Foundation of China (81830058, 11971296) and the 111 Project (D20031). (Corresponding authors: Jun Shi)

J. Shi, Y. Zhang, Z. Li, X. Han, S. Ding and J. Wang are with the Key Laboratory of Specialty Fiber Optics and Optical Access Networks, Joint International Research Laboratory of Specialty Fiber Optics and Advanced Communication, Shanghai Institute for Advanced Communication and Data Science, School of Communication and Information Engineering, Shanghai University, China. (Email: junshi@shu.edu.cn)

S. Ying is with the Department of Mathematics, School of Science, Shanghai University, China.

promote the CAD model to learn more specific properties of each center's data and further improve the generalization ability.

However, the pseudo histopathological images do not have corresponding labels for cancers, and therefore, they cannot be directly used to train the backbone network of a CAD model. Self-supervised learning (SSL) then provides a feasible way to capture and learn inherent information from these pseudo histopathological images, because it generates supervision directly from the training samples themselves to design pretext tasks [22][23]. SSL can effectively improve the feature representation of a backbone network for the downstream task, and it has been successfully applied to various tasks in the field of medical image analysis [24][25]. Consequently, we can develop an SSL-based FL framework to make full use of the pseudo histopathological images. That is, the backbone network of a CAD model will be pre-trained by conducting suitable SSL pretext tasks on these pseudo histopathological samples, which is then used as the initial global model for FL with learned inherent and specific information.

On the other hand, a recently proposed FL algorithm, namely Model-Contrastive Federated Learning (MOON), innovatively introduces contrastive SSL into FL for model-level contrast [26]. MOON adopts the similarity between model representations to correct the local training of individual centers, and it has achieved superior performance in handling the heterogeneity of local data distribution [26]. However, when MOON maximizes the representation agreement between the local and global models, the contrastive operation is still inefficient due to the requirements of negative samples similar to SimCLR [27]. As a new competitive contrastive SSL algorithm, Barlow Twins (BT) proposes a contrastive objective function based on the cross-correlation matrix by minimizing the redundancy between the components of the output vectors [28]. Compared to the contrastive operation in MOON, BT is more robust to the training batch size without any negative samples. It also avoids other trivial implementations, such as asymmetric mechanisms and momentum encoders [29], which are common in other contrastive SSL works but obviously not suitable for FL. Therefore, BT has the potential to be integrated into FL to conduct model-level contrast for improving local training of individual centers.

In this work, a novel SSL-based FL (SSL-FL) framework is proposed to improve the performance of CAD model for histopathological images. Specifically, the pseudo histopathological images are firstly generated in each center, which are fed to the multi-task SSL model to pre-train the backbone as the initial global model for further FL. The BT-based FL (FL-BT) algorithm is then proposed to further effectively train the CAD models for each center with improved performance. The experimental results on three public histopathological image datasets indicate the effectiveness of the proposed SSL-based FL-BT (SSL-FL-BT).

The main contributions of this work are three-fold as follows:

- 1) A novel SSL-based FL framework is proposed to improve both the diagnostic accuracy and generalization of a CAD model for histopathological images. In particular, we propose to generate pseudo histopathological images from each center, which are then shared for the pre-training backbone network. Thus, SSL can capture and learn both

the inherent and specific properties of data from different centers to benefit the generalization of the CAD model.

- 2) A multi-task SSL is further developed driven by the characteristics of pseudo histopathological images for the pre-training backbone network of a CAD model. Specifically, a source-center classification task is designed to judge which center the pseudo data come from, and the image restoration task is adopted to learn the common information of all data. This way of multiple pretext tasks promotes capturing more both specific and common inherent information from multi-center pseudo histopathological images.
- 3) A new FL-BT algorithm is proposed to improve the performance of local CAD model in each individual center. FL-BT integrates a cross-correlation matrix-based contrastive objective into FL to conduct model-level contrastive SSL. It not only minimizes the representation gaps between the local and global models to correct the local training, but also avoids other common trivial implementations in contrastive SSL.

II. RELATED WORK

A. SSL for CAD of Histopathological Images

Over the last years, the fast development of deep learning has made breakthroughs in the field of CAD for histopathological images [3]. According to the size of histopathological images, the current works are developed for the whole-slide images (WSI) and patches from WSIs [4], respectively. Based on the methodological aspect of different machine learning strategies, various deep learning algorithms for pathology CAD can be divided into the following categories: supervised, weakly supervised, unsupervised, transfer learning and other sub-variants [30]. Although lots of deep learning algorithms have been proposed in this field, they should be further improved due to the complexity of histopathological images and a variety of cancers.

Since it is time-consuming to annotate a large number of histopathological images for CAD, SSL represents an especially promising approach to alleviate this problem by pre-training the model under the supervision of the data itself. For example, Hu et al. proposed a unified generative adversarial network to learn robust cell-level representation for classification of histopathological images [31]; Stack et al. applied the contrastive predictive coding to histopathology datasets, indicating that the low-level features were more effective for tumor classification [32]; Ciga et al. utilized SimCLR to pre-train the model on multiple histopathological datasets, which improved the performances on different downstream CAD tasks [33]. All these works demonstrate the effectiveness of SSL for CAD with limited histopathological images.

It is worth noting that the application of SSL should not only retain the center-specific information, but also mine more inherent common features from the data of all centers for FL in our task. However, the single pretext task generally cannot well explore this information. To this end, multi-task SSL has the potential to learn more comprehensive features from training

samples. In the pioneering work, Koohbanani et al. proposed a multi-task SSL algorithm Self-Path for histopathological images, which included three pathology-specific tasks, *i.e.*, magnification prediction, magnification Jigsaw puzzle, and Hematoxylin channel prediction, to improve the model performance with limited annotations [33]. Since Self-Path can achieve superior performance over the single-task based approaches, we will also specifically design a multi-task SSL according to the data characteristics of multi-center histopathological images.

B. Federated Learning

FL is an emerging distributed learning method, which aims to share the local model parameters in a parallel manner instead of the conventional local data[12]. Due to the advantages of both privacy-preserving and distributed optimization, FL has been successfully applied to many fields [13], such as financial, smart retail and healthcare. FedAvg is the first FL algorithm that aggregates the local models by averaging the model weights [35]. Recently, some variants of Fed-Avg have been proposed, which mainly include the following two methods: 1) Local training methods, such as FedProx [36], SCAFFOLD [37] and MOON [26]; 2) Aggregation method, such as FedNova [38], FedMA [39], FedAvgM [40] and Auto-FedAvg [41]. All these works show the effectiveness of FL for multiple center learning.

FL is particularly attractive for CAD now [18]. It can not only improve the generalization of CAD models, but also alleviate the SSS issue by collecting multi-center data with privacy protection. Some pioneering works have been conducted. For example, Li *et al.* proposed an FL algorithm for diagnosing the autism spectrum disorders with multi-site fMRI data, in which decentralized iterative optimization and randomization mechanism were used [16]; Andreux et al. introduced a local statistical batch normalization layer in the model architecture of FL, which was applied to the diagnosis of breast tumor with multi-centric histopathology datasets [42]; Yang et al. proposed an FL algorithm using partial networks for COVID-19 diagnosis with multiple X-ray datasets [17]. These works indicate that FL can effectively improve the model performance in local servers together with privacy-preserving.

However, the existing FL methods cannot sufficiently handle the gap between the local models and the central model, in which some implementations, such as trivial implementations, such as asymmetric mechanisms and momentum encoders, are still involved. Therefore, its learning performance is limited.

III. METHODOLOGY

Fig. 1 shows the overall pipeline of the proposed SSL-FL-BT, which includes two stages, *i.e.*, SSL stage and FL stage. In the SSL stage, the pseudo histopathological images are firstly generated in each center with a GAN. The specially designed multi-task SSL is then performed on all the pseudo images to pre-train the backbone network. Here, the source-center classification and image restoration tasks are designed as the multiple pretext tasks, and both tasks share the backbone. The pre-trained backbone is then used as the initialization network

in the subsequent FL stage, and it is trained by the proposed FL-BT with multi-center real histopathological images. In the testing stage, a histopathological image is fed to the corresponding CAD model in a center for cancer diagnosis.

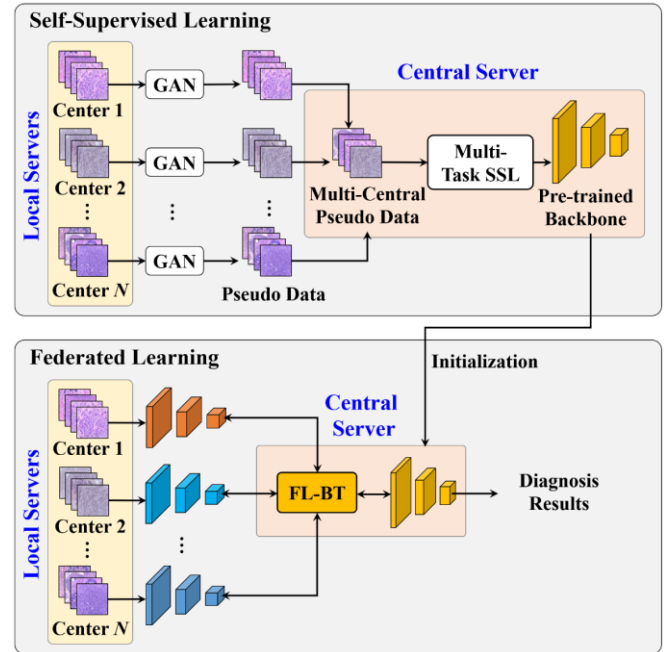


Fig. 1. The pipeline of the proposed SSL-FL-BT.

A. Multi-task SSL for FL

Since the stained histopathological images have inconsistencies among different centers, we propose to share the pseudo histopathological images without privacy information for FL, which can provide more heterogeneous center-specific information of each center for the CAD model, and further improve its generalization. Here, we specifically design a multi-task SSL to capture and learn both the center-specific information and common inherent representation according to the data characteristics of multi-center pseudo histopathological images. The overall pipeline of our proposed multi-task SSL is shown in Fig. 2.

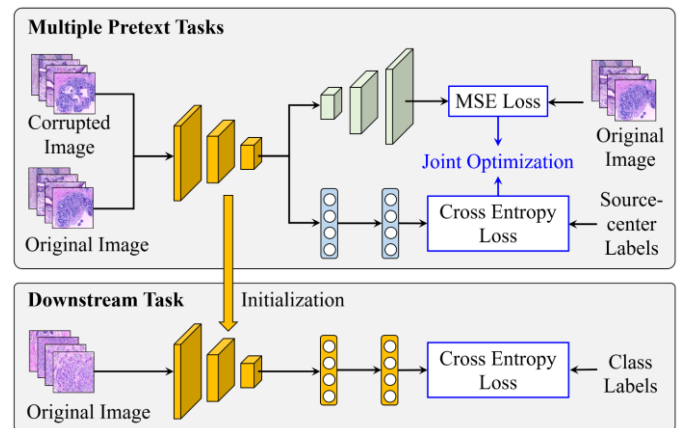


Fig. 2. The pipeline of the proposed multi-task Self-supervised learning.

As shown in Fig. 2, the pseudo data are firstly generated in each center through the GAN model, which are then shared to

the server for pre-training backbone network by SSL. Two pretext tasks are then designed, *i.e.*, the source-center classification task and image restoration task. The former pretext task predicts which center the synthetic data belong to. It can explore more specific properties of data in each center. While the latter pretext task restores the corrupted images to their original pseudo images, which can learn more inherent information of the data collected from different centers.

Pseudo Image Generation: In order to generate high-fidelity pseudo histopathological images, the multi-scale gradient generative adversarial network (MSG-GAN) algorithm is adopted in this work, which provides high-quality synthesized images for the following multi-task SSL [42].

MSG-GAN introduces a multiscale gradient technique that allows the gradients flow to propagate from the discriminator to the generator at multiple scales. This technique improves the stability of training for image synthesis on data with different sizes, resolutions, and domains. Compared to other GANs and their variants, MSG-GAN can boost the performance in most of cases. The detailed information about the MSG-GAN can be referred to [42].

The generated real and pseudo examples of histopathological images are shown in Fig. 3.

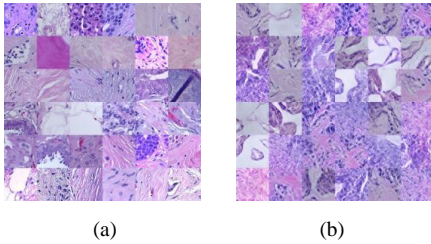


Fig. 3: (a) Real histopathological images; (b) Pseudo histopathological images.

Multiple Pretext Tasks: Two SSL pretext tasks are developed based on the characteristics of pseudo histopathological images for pre-training backbone, *i.e.*, the source-center classification task and image restoration task.

The source-center classification task tries to predict which source-center a pseudo image is generated from, and thus the center identity document (ID) is considered as the labels. Since the pseudo images are generated based on each center's data, these images contain center-specific information extracted from the real histopathological images of the corresponding center. Thus, this pretext task can effectively learn the heterogeneous characteristics pseudo images generated from each center.

The SSL image restoration task is designed to extract detailed context information and high-level representation in histopathological images, which contain the common characteristics across centers. Specifically, we randomly swap patches in the original pseudo images to generate the corrupted versions, like the operation in an image restoration based SSL [24]. These corrupted images are then fed to the backbone network to restore the original pseudo images as ground truths.

To conduct two pretext tasks in a unified framework with a single shared network, the hard parameter sharing is utilized to construct a multi-task learning architecture [44]. In our implementation, the commonly used ResNet50 is used as the shared backbone, followed by a classification branch and a

reconstruction head [45].

For the source-center classification task, the cross-entropy (CE) loss L_{CE} is utilized for the SSL classification task, which can be given as follows:

$$L_{CE} = -\frac{1}{N} \sum_i \sum_{c=1}^M y_{ic} \log(P_{ic}) \quad (1)$$

where $y_{ic} \in \{0,1\}$ is an indicator that returns 1 if and only if the i -th self-assigned label is c . P_{ic} denotes the probability that the category of the i -th sample is c .

For the image restoration task, the mean squared error (MSE) is adopted as the objective function for the SSL image restoration task. Given a corrupted image I_i and the reconstruction sub-network $G(\cdot)$, the MSE loss is formulated as:

$$L_{MSE} = \frac{1}{N} \sum_{i=1}^N \|G(I_i) - x_i\|^2 \quad (2)$$

where $G(I_i)$ and x_i denote the restored image and the corresponding ground truth, respectively.

The overall loss L_{SSL} for our multi-task SSL is then formulated as:

$$L_{SSL} = L_{CE} + L_{MSE} \quad (3)$$

The pre-trained backbone is then used as the initialization for the followed FL stage. This multi-task SSL strategy can capture both the specific and common inherent information from the multi-center pseudo histopathological images.

B. FL-BT for Histopathological Images

The generalization of a CAD model for histopathological images is generally limited by the training samples only from a single center, because the stained images have different data distributions in different hospitals. FL can improve both the diagnostic accuracy and generalization ability of CAD models with multi-center histopathological images, while private information can also be protected [50].

The existing FL methods cannot well handle the heterogeneity of multiple local data distribution. MOON is proposed to address this issue, which adopts the similarity among model representations to correct the local training of individual centers [26]. However, the robustness of MOON should be further improved, since the trivial implementations are applied in the local training process. To this end, we propose a novel FL-BT to train the CAD model with multi-center histopathological images.

Suppose there are N centers, which are denoted as C_1, \dots, C_N . Center C_i has a local dataset \mathcal{D}_i with histopathological images $x_i, i = 1, 2, \dots, N$. The proposed FL-BT aims to learn a model w_i over the local dataset \mathcal{D}_i with the help of a global model w^g in central server.

Network Architecture of Local Model: The architecture of each local network for FL-BT is shown in Fig. 4, which consists of a base encoder, a projector network, and an output layer. The base encoder is the widely used ResNet50, which learns the feature representation from input real histopathological images. The projector network is then adopted to map the representation to a feature space with a fixed dimension. Finally, the output layer is used to predict the classification results for each cancer class.

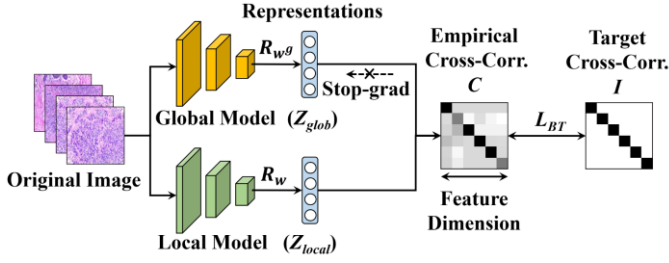


Fig. 4: Flowchart of the FL-BT algorithm.

Local Training: Our algorithm works under the assumption that local training is performed in each center C_i . The pre-trained global model trained by multi-task SSL is set as the initial model w_i in center C_i . The input data x is used to generate two distorted vires A and B , which are fed to the base encoder to generate feature representations Z_A and Z_B , respectively. After that, the projector network maps the Z_A and Z_B to the fixed dimension. Finally, the classification results are predicted by the output layer.

The local objective function contains two parts: \mathcal{L}_{sup} and \mathcal{L}_{FL-BT} . The former part \mathcal{L}_{sup} is a cross-entropy loss in the supervised learning manner, while the second part \mathcal{L}_{FL-BT} is the contrastive loss in our proposed FL-BT.

Specifically, the supervision loss \mathcal{L}_{sup} in FL-BT can be given as:

$$L_{sup} = \text{CrossEntropyLoss}(F_{w_i}(x), y) \quad (4)$$

While the contrastive loss \mathcal{L}_{FL-BT} designed in FL-BT can be formulated as:

$$L_{FL-BT} = \sum_i (1 - C_{ii})^2 + \lambda \sum_i \sum_{j \neq i} C_{ij}^2 \quad (5)$$

where λ is the weight to trade off the importance of the first and second terms; C_{ij} denotes the cross-correlation matrix, which is computed between the outputs of the two branches along the batch dimension; both i, j represent the dimensions of the networks' output vectors. More specifically, C_{ij} can be calculated as follows:

$$C_{ij} = \frac{\sum_b z_{local}^{b,i} z_{glob}^{b,j}}{\sqrt{\sum_b (z_{local}^{b,i})^2} \sqrt{\sum_b (z_{glob}^{b,j})^2}} \quad (6)$$

where the superscript b denotes batch samples and C_{ij} is a square matrix with size the dimensionality of the network's output.

To this end, the definition of the whole loss function can be given by:

$$L = L_{sup}(w_i; (x_i, y_i)) + \mu \mathcal{L}_{FL-BT}(w_i; w^g; (x_i, y_i)) \quad (7)$$

where μ is the factor to balance the weight of contrastive loss \mathcal{L}_{FL-BT} .

And the local objective is to minimize:

$$\min_{w_i} \mathbb{E}_{(x,y) \sim \mathcal{D}_i} [L_{sup}(w_i; (x_i, y_i)) + \mu \mathcal{L}_{FL-BT}(w_i; w^g; (x_i, y_i))] \quad (8)$$

In local training, each model uses stochastic gradient descent to update the parameters with the local data, the objective is shown in Eq. (4).

Global Aggregation: After the local training in each center, the updated parameters w_i , which $i = 1, \dots, N$, in local models are then sent to the central server to implement the model aggregation.

FL-BT seeks to minimize the following objective function for model training:

$$\min_w L(w) = \sum_{i=1}^N \alpha_i L_i \quad (9)$$

where N denotes the number of the centers, α_i denotes the importance of the i -th center, and $\sum_i \alpha_i = 1$. L_i denotes the whole loss in Eq. (4) for i -th center.

In this work, we adopt the classical FedAvg as the aggregation method [35], in which w_i are averaged as the global model w^g . In communication round t , the updated parameters for the global model can be formulated as the follows:

$$w_g \leftarrow \sum_{i=1}^N \frac{m_i}{M} w_i \quad (10)$$

where m_i denotes the number of images in center i , and M denotes the total number of images.

Then, the updated parameters of the global model w^g is deployed to all the local servers, the updated parameters for the local model can be formulated as:

$$\forall_i w_{g+1} \leftarrow w_g - \eta g_i \quad (11)$$

where η denotes the learning rate for model optimization and g_i denotes the gradients at each local model. The final model is obtained after several communication rounds.

The detailed scheme of FL-BT is shown in Algorithm 1.

Algorithm 1: The FL-BT framework

Input: local datasets, number of communication rounds T , number of local epochs E , number of classes, number of clients N , learning rate η

Output: The final model w^T

1: **Server executes:**

2: initialize w

3: **for** $t = 0, 1, \dots, T - 1$ **do**

4: **for** $i = 1, 2, \dots, N$ **in parallel do**

5: send the global model w^g to C_i

6: $w_i \leftarrow \text{PartyLocalTraining}(i, w^g)$

7: $w^{g+1} \leftarrow \sum_{k=1}^N \frac{m_k}{M} w_k^g$

8: return w^T

9: **PartyLocalTraining**(i, w^g):

10: $w_i \leftarrow w^g$

11: **for** epoch $i = 1, 2, \dots, E$ **do**

12: **for each batch** $\mathbf{b} = \{x, y\}$ **of** \mathcal{D}^i **do**

13: $l_{sup} \leftarrow \text{CrossEntropyLoss}(F_{w_i}(x), y)$

14: $z \leftarrow R_{w_i}(x)$

15: $z_{glob} \leftarrow R_{w^g}(x)$

16: $\mathcal{L}_{FL-BT} \leftarrow \sum_i (1 - C_{ii})^2 + \lambda \sum_i \sum_{j \neq i} C_{ij}^2$

17: $l \leftarrow l_{sup} + \mu \mathcal{L}_{FL-BT}$

18: $w_i \leftarrow w_i - \eta \nabla l$

19: **return** w_i **to server**

BT is more robust to the training batch size without any negative samples. It also avoids other trivial implementations, such as asymmetric mechanisms and momentum encoders, which are common in other contrastive SSL works, but obviously not suitable for FL.

IV. EXPERIMENTS AND RESULTS

A. Datasets and Data Preprocessing

The proposed algorithm was evaluated on three public breast histopathological datasets: the 2015 Bioimaging Challenge Dataset [46], the 4th Symposium in Applied Bioimaging Dataset [47], and the ICIAR 2018 Grand Challenge on Breast Cancer Histology Images Dataset [48]. Since all the datasets had the same classes, *i.e.*, normal tissues, benign lesions, in situ carcinomas, and invasive carcinomas, these datasets were then considered as three centers in this work. In our experiments, the 2015 Bioimaging Challenge Dataset, the 4th Symposium in Applied Bioimaging Dataset and the ICIAR 2018 Grand Challenge on Breast Cancer Histology Images Dataset were considered as Center 1 (C1), Center 2 (C2) and Center 3 (C3), respectively.

The detailed information about the three datasets is given in Table I. All the histopathological images were stained by hematoxylin and eosin (H&E). Fig. 5 shows some example images from three datasets.

TABLE I
DETAILED INFORMATION ABOUT THE THREE DATASETS

Datasets	Classes/Numbers	Center
2015 Bioimaging Challenge Dataset	Normal Tissues:64 Benign Lesions:78 In Situ Carcinomas:72 Invasive Carcinomas:71	Center 1
The 4th Symposium in Applied Bioimaging Dataset	Normal Tissues:30 Benign Lesions:30 In Situ Carcinomas:30 Invasive Carcinomas:30	Center 2
ICIAR 2018 Grand Challenge	Normal Tissues:100 Benign Lesions:100 In Situ Carcinomas:100 Invasive Carcinomas:100	Center 3

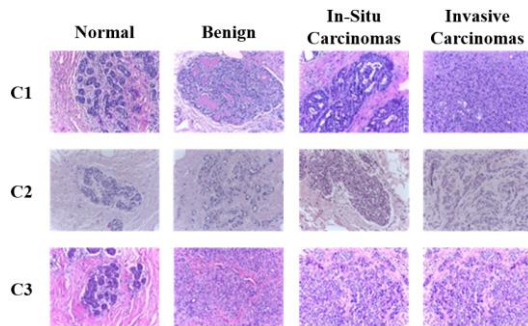


Fig. 5: The histopathological images in three datasets.

B. Experimental Setup

To validate the effectiveness of the proposed SSL-FL-BT, the following related algorithms were compared:

- 1) ResNet50 [45]: The ResNet50 was directly trained only with the histopathological images from one center, which

was a single-center based CAD without FL.

- 2) FedAvg [35]: FedAvg was selected for comparison as a classical FL algorithm, which utilized fixed weights to average the local models for the optimization of the global model.
- 3) FedProx [36]: FedProx was also selected for comparison as a classical FL algorithm, which added a proximal term in the aggregation method proposed by FedAvg to stabilize the convergence.
- 4) FedBN [49]: FedBN was compared as a state-of-the-art FL algorithm, which aggregated the local models without sharing parameters in BN layers to obtain the global model.
- 5) MOON [26]: MOON was compared as the contrastive learning-based FL algorithm, which adopted contrastive learning to reduce the gaps between the local models and the global model.

It is worth noting that all the compared algorithms adopted ResNet50 as the backbone.

On the other hand, an ablation experiment was conducted to evaluate the effectiveness of the multi-task SSL in SSL-FL by comparing SSL-FL-BT with the following algorithms:

- 1) FL-BT: FL-BT directly trained the CAD models of all centers without the pre-trained backbone by multi-task SSL.
- 2) SSL-C-FL-BT: This algorithm only designed the source-center classification task as the pretext task for SSL, and then conducted the SSL-based FL.
- 3) SSL-R-FL-BT: This algorithm only designed the restoration task as the pretext task for SSL, and then conducted the SSL-based FL.

The five-fold cross-validation strategy was applied to all algorithms on three datasets. The commonly used classification accuracy, precision, recall, and F1-score were selected as evaluation indices, which were computed as follows:

$$\begin{cases} Accuracy = \frac{TP+TN}{TP+TN+FP+FN} \\ Precision = \frac{TP}{TP+FP} \\ Recall = \frac{TP}{TP+FN} \\ F1 = 2 \times \frac{Precision \times Recall}{Precision+Recall} \end{cases} \quad (12)$$

where TP is the number of true positive, TN is the number of true negative, FP is the number of false positive and FN is the number of false negative. The results were reported in the format of mean \pm SD (standard deviation). The precision-recall (PR) curve and average precision (AP) were also used to evaluate the performance.

Moreover, the value of global test average (GTA) was used to quantitatively measure the generalization ability of the global model [41], which computed the average accuracy, precision, recall and F1-score values on the results of three centers, respectively.

C. Implementation Details

All histopathological images were resized to 256 \times 256 for model training. MSG-GAN was used for pseudo images generation. The learning rate for the generator and discriminator was 0.003, while the number of epochs for training was 100. Each center generated 1000 images with the

size of 256×256 . Data augmentation was conducted on all datasets for all algorithms, including rotation (90° , 180° , 270°) and horizontally flipping.

ResNet50 was adopted as the backbone for multi-task SSL and FL. For each FL algorithm, the model was trained for 300 rounds of 1 local epoch using a batch size of 4. The weight μ for contrastive loss in Eq. (4) was set to 0.01, while the trade-off weight λ in Eq. (7) was set to 0.005. The stochastic gradient descent (SGD) was used for the optimization of each algorithm with the learning rate of 0.001. All algorithms were implemented on Pytorch.

D. Results on Multi-Center Datasets

Table II shows the results of different algorithms on C1. It can be found that all the FL algorithms achieve superior performances to ResNet50, which is a single-center based approach trained only with the data of C1. It indicates that FL algorithms can effectively improve the performances of a CAD model with multi-center data. Moreover, the proposed SSL-FL-BT outperforms all the compared FL algorithms on all indices with the best mean classification accuracy of $96.06 \pm 0.57\%$, precision of $96.21 \pm 0.46\%$, recall of $96.15 \pm 0.53\%$ and F1-score of $96.03 \pm 0.56\%$. It improves at least 3.82%, 3.33%, 3.65% and 3.73% on accuracy, precision, recall and F1-score, respectively, compared to FedAvg, FedProx, FedBN and MOON, suggesting that both multi-task SSL and FL-BT effectively improve the performance. On the other hand, it also can be observed that the proposed FL-BT achieves the second-best results, and gets the improvements of 1.18%, 1.16%, 1.14% and 1.17% on the corresponding indices, respectively, compared to other FL algorithms except for our proposed SSL-FL-BT, which demonstrates the effectiveness of BT in the proposed FL-BT.

Table III shows the results of different algorithms on C2. The FL algorithms still achieve better performances than those of the ResNet50-based CAD only using the training images in C2. Specifically, our proposed SSL-FL-BT gains the best results of $96.66 \pm 1.86\%$, $97.14 \pm 1.60\%$, $96.66 \pm 1.86\%$ and $96.64 \pm 1.88\%$ on the accuracy, precision, recall and F1-score, respectively, which improves at least 4.16%, 3.03%, 4.16%, and 4.39%, on the corresponding indices, respectively, compared to other FL algorithms. The FL-BT again achieves the second-best performance by improving at least 1.67%, 1.25%, 1.67%, and 1.80% on the accuracy, precision, recall and F1-score, respectively, over other compared FL algorithms.

Table IV gives the results of different algorithms on C3, which demonstrate similar trends to those in Table II and Table III. SSL-FL-BT again achieves the best results of $94.50 \pm 0.68\%$, $94.85 \pm 0.83\%$, $94.50 \pm 0.68\%$ and $94.46 \pm 0.69\%$ on the accuracy, precision, recall and F1-score, respectively, which improves 3.25%, 3.64%, 3.25%, and 3.21% on the corresponding indices, respectively, compared to FedAvg, FedProx, FedBN and MOON. Besides, The FL-BT is the second to SSL-FL-BT, and outperforms all the other compared FL algorithms. All these results suggest the effectiveness of our proposed SSL-FL-BT.

Fig. 6 shows the PR curves and the corresponding AP values for different algorithms. The proposed SSL-FL-BT achieves the best AP value of 0.9864 on C1, 0.9703 on C2 and 0.9591 on C3, which again indicates its effectiveness.

TABLE II
CLASSIFICATION RESULTS OF DIFFERENT ALGORITHMS ON C1 (UNIT: %)

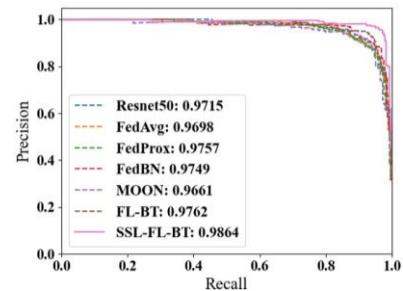
Algorithms	Accuracy	Precision	Recall	F1-score
ResNet50	89.26 \pm 2.33	90.31 \pm 2.68	89.21 \pm 2.08	89.26 \pm 2.24
FedAvg	90.83 \pm 1.50	91.84 \pm 1.79	90.83 \pm 1.56	90.73 \pm 1.65
FedProx	91.50 \pm 1.65	92.14 \pm 1.86	91.75 \pm 1.55	91.58 \pm 1.78
FedBN	91.84 \pm 1.42	92.48 \pm 1.55	92.08 \pm 1.41	91.92 \pm 1.56
MOON	92.24 \pm 1.70	92.88 \pm 1.66	92.50 \pm 1.56	92.30 \pm 1.84
FL-BT	93.42\pm1.33	94.04\pm1.52	93.64\pm1.22	93.47\pm1.46
SSL-FL-BT	96.06\pm0.57	96.21\pm0.46	96.15\pm0.53	96.03\pm0.56

TABLE III
CLASSIFICATION RESULTS OF DIFFERENT ALGORITHMS ON C2 (UNIT: %)

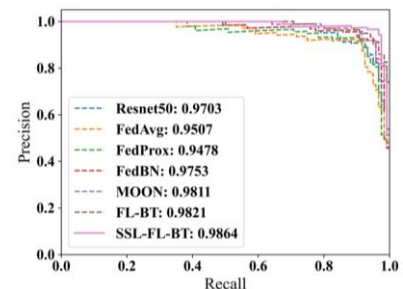
Algorithms	Accuracy	Precision	Recall	F1-score
ResNet50	85.83 \pm 3.73	87.27 \pm 3.34	85.83 \pm 3.73	85.65 \pm 3.76
FedAvg	90.84 \pm 1.86	92.15 \pm 2.81	90.84 \pm 1.86	90.60 \pm 1.97
FedProx	91.67 \pm 2.95	93.39 \pm 2.24	91.67 \pm 2.95	91.41 \pm 3.03
FedBN	92.50 \pm 3.48	93.52 \pm 3.75	92.50 \pm 3.48	92.31 \pm 3.65
MOON	92.50 \pm 1.86	94.11 \pm 1.35	92.50 \pm 1.86	92.25 \pm 1.99
FL-BT	94.17\pm1.86	95.36\pm1.47	94.17\pm2.28	94.05\pm2.39
SSL-FL-BT	96.66\pm1.86	97.14\pm1.60	96.66\pm1.86	96.64\pm1.88

TABLE IV
CLASSIFICATION RESULTS OF DIFFERENT ALGORITHMS ON C3 (UNIT: %)

Algorithms	Accuracy	Precision	Recall	F1-score
ResNet50	89.75 \pm 2.05	90.45 \pm 1.88	89.75 \pm 2.05	89.74 \pm 2.14
FedAvg	90.00 \pm 2.65	91.11 \pm 2.46	90.00 \pm 2.65	90.00 \pm 2.58
FedProx	90.25 \pm 2.05	90.98 \pm 1.82	90.25 \pm 2.05	90.18 \pm 2.08
FedBN	90.75 \pm 2.88	91.54 \pm 2.50	90.75 \pm 2.88	90.78 \pm 2.77
MOON	91.25 \pm 1.53	91.21 \pm 1.37	91.25 \pm 1.53	91.25 \pm 1.41
FL-BT	92.50\pm0.88	93.02\pm1.11	92.50\pm0.88	92.47\pm0.88
SSL-FL-BT	94.50\pm0.68	94.85\pm0.83	94.50\pm0.68	94.46\pm0.69



(a) C1



(b) C2

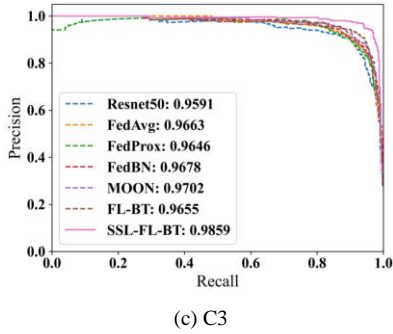


Fig. 6. PR curves of the compared algorithms with the corresponding AP values on the datasets of (a) C1, (b) C2, and (c) C3.

E. Results of Ablation Experiments

Table V shows the results of the ablation experiments on C1. Both the SSL-C-FL-BT and SSL-R-FL-BT improve their performances compared to FL-BT, indicating that the single pretext task, namely source-center classification task or image restoration task, effectively improves the feature representation of backbone. Therefore, the final diagnostic results are improved due to the pre-trained backbone compared with the original FL-BT. Moreover, SSL-C-FL-BT achieves a little better improvement compared to SSL-R-FL-BT, suggesting that the specific and heterogeneous information provided by the classification task can further assist the diagnosis. Besides, our proposed SSL-FL-BT achieves the best results by improving at least 1.65%, 1.22%, 1.62%, and 1.61% on the accuracy, precision, recall and F1-score, respectively. It demonstrates the effectiveness of the multi-task SSL framework in FL.

Table VI shows the results of the ablation experiments on C2, which has similar trends to the results in Table V. The SSL-C-FL-BT and SSL-R-FL-BT also achieve superior results compared to FL-BT, indicating the effectiveness of the self-designed pretext tasks. Moreover, our proposed SSL-FL-BT gets the improvements of at least 1.66%, 1.78%, 1.66%, and 1.72% on accuracy, precision, recall and F1-score, respectively, over other compared algorithms.

Similar results can also be observed in Table VII, which gives the results of the ablation experiments C3. SSL-FL-BT improves at least 0.75%, 0.55%, 0.75%, and 0.77% on accuracy, precision, recall and F1-score, respectively, compared to other ablation algorithms. All these results indicate the effectiveness of the proposed multi-task SSL in FL.

TABLE V
ABLATION EXPERIMENT RESULTS ON C1 (UNIT: %)

Algorithms	Accuracy	Precision	Recall	F1-score
FL-BT	93.42±1.33	94.04±1.52	93.64±1.22	93.47±1.46
SSL-C-FL-BT	94.41±1.55	94.99±1.32	94.53±1.22	94.42±1.58
SSL-R-FL-BT	94.16±2.29	94.75±2.19	94.36±2.18	94.20±2.36
SSL-FL-BT	96.06±0.57	96.21±0.46	96.15±0.53	96.03±0.56

TABLE VI
ABLATION EXPERIMENT RESULTS ON C2 (UNIT: %)

Algorithms	Accuracy	Precision	Recall	F1-score
FL-BT	94.17±1.86	95.36±1.47	94.17±2.28	94.05±2.39
SSL-C-FL-BT	95.00±1.86	95.36±1.20	95.00±1.86	94.92±1.95
SSL-R-FL-BT	95.00±3.48	96.07±2.57	95.00±3.48	94.89±3.60
SSL-FL-BT	96.66±1.86	97.14±1.60	96.66±1.86	96.64±1.88

TABLE VII
ABLATION EXPERIMENT RESULTS ON C3 (UNIT: %)

Algorithms	Accuracy	Precision	Recall	F1-score
FL-BT	92.50±0.88	93.02±1.11	92.50±0.88	92.47±0.88
SSL-C-FL-BT	93.75±1.53	94.30±1.37	93.75±1.53	93.69±1.49
SSL-R-FL-BT	93.50±1.85	93.91±1.94	93.50±1.85	93.42±1.84
SSL-FL-BT	94.50±0.68	94.85±0.83	94.50±0.68	94.46±0.69

F. Generalization and Robustness Analysis

Fig. 7 shows the GTA results of different algorithms. It can be found that all the FL algorithms achieve superior GTA values to ResNet50, suggesting that the FL strategy can effectively improve the generalization of CAD models with multi-center data. Moreover, the proposed SSL-FL-BT algorithm achieves the best GTA values with the mean accuracy of 95.74±1.43%, precision of 96.06±0.96%, recall of 95.77±1.02% and F1-score of 95.71±1.44%. It improves at least 3.75%, 3.33%, 3.69% and 3.78% on the corresponding indices, respectively, over FedAvg, FedProx, FedBN and MOON.

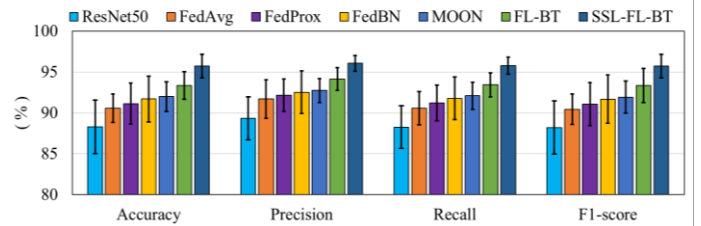


Fig. 7. Histogram chart of the GTA for the compared algorithms.

Moreover, as shown in Fig. 7, the proposed SSL-FL-BT achieves the lowest standard deviation on all indices, indicating SSL-FL-BT has better robustness and generalization.

V. DISCUSSION

In this work, a novel SSL-FL-BT framework is proposed to promote both the diagnostic accuracy and generalization ability of the CAD model for histopathological images. The experimental results on three public datasets have validated the effectiveness of the proposed SSL-FL-BT.

The stain of histopathological images is generally affected by several factors, such as the brand, storage time, and temperature, which result in the inconsistencies of histopathological images across different hospitals. It then degrades the generalization ability of the CAD model, if this model is only trained with the data acquired from a single center. On the other hand, it is generally time-consuming and expensive to collect large amounts of annotated data in one center, and therefore, the SSS problem is common in the field of CAD. Multi-center learning is an effective way to alleviate both issues, which trains the model by collecting data from different centers. It can not only enrich the variety of histopathological images, but also enhance the training set. Therefore, the multi-center learning based CAD is more feasible to meet the clinical requirement than the single-center based approach, and it can effectively improve both the diagnostic accuracy and generalization ability.

The conventional multi-center learning paradigm suffers from the challenges of privacy protection and data security,

because it gathers all data across centers. On the contrary, FL jointly trains the CAD models by sharing parameters of distributed local models instead of the local data in the conventional multi-center learning paradigm. Therefore, this multi-center learning paradigm guarantees privacy protection for multi-center histopathological images. The experimental results in Table II to IV demonstrate that FL algorithms achieve superior performances to the CAD model trained only using single-center data, and also protect the private information. Therefore, FL has the feasibility to be applicable in other multi-center medical applications.

Although FL has the advantage of privacy protection, it still cannot guarantee that the distributed CAD models fully capture the center-specific information from each center's data to further improve generalization, because it does not share the data from different centers. In this work, we propose to generate pseudo histopathological images from different centers for this issue. These self-generated pseudo images contain center-specific inherent properties corresponding to the original images of each center, respectively, but do not have private information. Therefore, these pseudo images can be shared in the central server. Two SSL pretext tasks are then designed based on the characteristics of pseudo images for the pre-training backbone. The source-center classification task tries to learn the heterogeneous properties of each center, and the image restoration task aims to capture common characteristics across centers. The results in Table V, Table VI, and Table VI show that the classification task can better promote the performance compared to the restoration task. It seems that the center-specific information is more helpful for the generalization of a CAD model. Besides, the combination of two tasks achieves significant improvement compared with the single task, demonstrating the effectiveness of multi-task SSL driven by the properties of multi-center data themselves.

In addition, we propose an effective algorithm, namely FL-BT, to improve the classification performance of local training. FL-BT utilizes the similarity between model representations to minimize the representation redundancy of the local model, which benefits the optimization of the global model in the FL procedure. The loss function in FL-BT consists of two parts, *i.e.*, the invariance term and redundancy reduction term. The former plays a role in bringing the positive examples closer to each other in the representation space, while the latter enhances the independence of each element of the vector. Compared with the conventional contrastive SSL algorithms, which require positive and negative samples to conduct contrastive learning, the proposed FL-BT eliminates the redundant information expression in the representation vector as much as possible. The subterm acts like negative samples, avoiding model collapse. Therefore, FL-BT achieves superior performance.

Although the results on three public datasets indicate the superior performance of the proposed SSL-FL-BT framework, we will further evaluate it with more centers' data in future work. Besides, the proposed CAD model performs the patch-level diagnosis for histopathological images in this work. It will be extended to the version for the WSIs, which is more difficult

due to the SSS problem. On the other hand, the current pseudo-data based SSL is performed on the central server, and it can be further improved with the SSL training manner by combining both the central server and distributed clients.

VI. CONCLUSION

In this work, a novel pseudo-data based SSL-FL-BT framework is proposed to improve both the diagnostic accuracy and generalization of the CAD model for histopathological images. The self-generated pseudo images contain inherent and center-specific properties corresponding to the real histopathological images of each center without privacy information, while the self-designed multi-task SSL captures both the representation from these pseudo images for the pre-trained backbone network. The proposed FL-BT further promotes the performance of the CAD model. The experimental results on three public histopathological image datasets indicate the effectiveness of the proposed SSL-FL-BT.

REFERENCES

- [1] M. N. Gurcan, L. E. Boucheron, A. Can, A. Madabhushi, N. M. Rajpoot, and B. Yener, "Histopathological image analysis: A review," *IEEE Rev. Biomed. Eng.*, vol. 2, pp. 147-171, 2009.
- [2] M. Veta, J. P. Pluim, P. J. Van Diest, and M. A. Viergever, "Breast cancer histopathology image analysis: A review," *IEEE Trans. Biomed. Eng.*, vol. 61, no. 5, pp. 1400-1411, 2014.
- [3] S. Deng, X. Zhang, W. Yan, E. I.-C. Chang, Y. Fan, M. Lai, and Y. Xu, "Deep learning in digital pathology image analysis: A survey," *Front. Med.*, vol. 14, no. 4, pp. 470-487, 2020.
- [4] C. L. Srinidhi, O. Ciga, and A. L. Martel, "Deep neural network models for computational histopathology: A survey," *Med. Image Anal.*, vol. 67, p. 101813, 2021.
- [5] J. Shi, X. Zheng, J. Wu, B. Gong, Q. Zhang, and S. Ying, "Quaternion Grassmann average network for learning representation of histopathological image," *Pattern Recognit.*, vol. 89, pp. 67-76, 2019.
- [6] J. Noorbakhsh, S. Farahmand, A. Foroughi pour, S. Namburi, D. Caruana, D. Rimm, M. Soltanieh-ha, K. Zarringhalam, and J. H. Chuang, "Deep learning-based cross-classifications reveal conserved spatial behaviors within tumor histological images," *Nat. Commun.*, vol. 11, no. 1, p. 6367, 2020.
- [7] Z. Gao, J. Shi, and J. Wang, "GQ-GCN: Group quadratic graph convolutional network for classification of histopathological images," in *Proc. Int. Conf. Med. Image Comput. Comput. Assist. Interv. (MICCAI)*, pp. 121-131, 2021.
- [8] Z. Gao, Z. Lu, J. Wang, S. Ying, and J. Shi, "A convolutional neural network and graph convolutional network based framework for classification of breast histopathological images," *IEEE J. Biomed. Health. Inf.*, pp. 1-11, 2022.
- [9] Z. Huang, H. Lei, G. Chen, H. Li, C. Li, W. Gao, Y. Chen, Y. Wang, H. Xu, G. Ma, and B. Lei, "Multi-center sparse learning and decision fusion for automatic COVID-19 diagnosis," *Appl. Soft Comput.*, vol. 115, p. 108088, 2022.
- [10] J. N. Kather, J. Krisam, P. Charoentong, T. Luedde, E. Herpel, C.-A. Weis, T. Gaiser, A. Marx, N. A. Valous, D. Ferber, L. Jansen, C. C. Reyes-Aldasoro, I. Zörnig, D. Jäger, H. Brenner, J. Chang-Claude, M. Hoffmeister, and N. Halama, "Predicting survival from colorectal cancer histology slides using deep learning: A retrospective multi-center study," *PLoS Med.*, vol. 16, no. 1, p. e1002730, 2019.
- [11] H. Pinckaers, B. van Ginneken, and G. Litjens, "Streaming convolutional neural networks for end-to-end learning with multi-megapixel images," *IEEE Trans. Pattern Anal. Mach. Intell.*, vol. 44, no. 3, pp. 1581-1590, 2022.
- [12] M. J. Sheller, B. Edwards, G. A. Reina, J. Martin, S. Pati, A. Kotrotsou, *et al.*, "Federated learning in medicine: Facilitating multi-institutional collaborations without sharing patient data," *Sci. Rep.*, vol. 10, no. 1, pp. 1-12, 2020.

- [13] Q. Yang, Y. Liu, T. Chen, and Y. Tong, "Federated machine learning: Concept and applications," *ACM Trans. Intell. Syst. Technol.*, vol. 10, no. 2, pp. 1-19, 2019.
- [14] M. Alazab, S. P. RM, P. M, P. K. R. Maddikunta, T. R. Gadekallu, and Q.-V. Pham, "Federated learning for cybersecurity: Concepts, challenges, and future directions," *IEEE Trans. Ind. Inf.*, vol. 18, no. 5, pp. 3501-3509, 2022.
- [15] D. C. Nguyen, Q.-V. Pham, P. N. Pathirana, M. Ding, A. Seneviratne, Z. Lin, O. Dobre, and W.-J. Hwang, "Federated learning for smart healthcare: A survey," *ACM Comput. Surv.*, vol. 55, no. 3, pp.1-37, 2022.
- [16] X. Li, Y. Gu, N. Dvornek, L. H. Staib, P. Ventola, and J. S. Duncan, "Multi-site fMRI analysis using privacy-preserving federated learning and domain adaptation: ABIDE results," *Med. Image Anal.*, vol. 65, p. 101765, 2020.
- [17] Q. Yang, J. Zhang, W. Hao, G. P. Spell, and L. Carin, "FLOP: Federated learning on medical datasets using partial networks," in *Proceedings of the 27th ACM SIGKDD Conference on Knowledge Discovery & Data Mining*, 2021, pp. 3845-3853.
- [18] M. Y. Lu, R. J. Chen, D. Kong, J. Lipkova, R. Singh, D. F. K. Williamson, *et al.*, "Federated learning for computational pathology on gigapixel whole slide images," *Med. Image Anal.*, vol. 76, p. 102298, 2022.
- [19] I. Goodfellow, J. Pouget-Abadie, M. Mirza, B. Xu, D. Warde-Farley, S. Ozair, *et al.*, "Generative adversarial nets," in *Proc. Adv. Neural Inf. Process. Syst. (NeurIPS)*, 2014, vol. 27.
- [20] T. Karras, S. Laine, and T. Aila, "A style-based generator architecture for generative adversarial networks," in *Proceedings of the IEEE/CVF Conference on Computer Vision and Pattern Recognition (CVPR)*, 2019, pp. 4401-4410.
- [21] T. Karras, S. Laine, M. Aittala, J. Hellsten, J. Lehtinen, and T. Aila, "Analyzing and improving the image quality of StyleGAN," in *Proceedings of the IEEE/CVF Conference on Computer Vision and Pattern Recognition (CVPR)*, 2020, pp. 8110-8119.
- [22] L. Jing and Y. Tian, "Self-supervised visual feature learning with deep neural networks: A survey," *IEEE Trans. Pattern Anal. Mach. Intell.*, vol. 43, no. 11, pp. 4037-4058, 2021.
- [23] X. Liu, F. Zhang, Z. Hou, L. Mian, Z. Wang, J. Zhang, and J. Tang, "Self-supervised learning: Generative or contrastive," *IEEE Trans. Knowl. Data Eng.*, pp. 1-20, 2021.
- [24] L. Chen, P. Bentley, K. Mori, K. Misawa, M. Fujiwara, and D. Rueckert, "Self-supervised learning for medical image analysis using image context restoration," *Med. Image Anal.*, vol. 58, p. 101539, 2019.
- [25] X. Chen, L. Yao, T. Zhou, J. Dong, and Y. Zhang, "Momentum contrastive learning for few-shot COVID-19 diagnosis from chest CT images," *Pattern Recognit.*, vol. 113, p. 107826, 2021.
- [26] Q. Li, B. He, and D. Song, "Model-contrastive federated learning," in *Proceedings of the IEEE/CVF Conference on Computer Vision and Pattern Recognition (CVPR)*, 2021, pp. 10713-10722.
- [27] T. Chen, S. Kornblith, M. Norouzi, and G. Hinton, "A simple framework for contrastive learning of visual representations," in *Proc. Int. Conf. Mach. Learn. (ICML)*, 2020, pp. 1597-1607.
- [28] J. Zbontar, L. Jing, I. Misra, Y. LeCun, and S. Deny, "Barlow twins: Self-supervised learning via redundancy reduction," in *Proc. Int. Conf. Mach. Learn. (ICML)*, 2021, pp. 12310-12320.
- [29] K. He, H. Fan, Y. Wu, S. Xie, and R. Girshick, "Momentum contrast for unsupervised visual representation learning," in *Proceedings of the IEEE/CVF Conference on Computer Vision and Pattern Recognition (CVPR)*, 2020, pp. 9729-9738.
- [30] V. Cheplygina, M. de Bruijne, and J. P. Pluim, "Not-so-supervised: A survey of semi-supervised, multi-instance, and transfer learning in medical image analysis," *Med. Image Anal.*, vol. 54, pp. 280-296, 2019.
- [31] B. Hu, Y. Tang, I. Eric, C. Chang, Y. Fan, M. Lai, *et al.*, "Unsupervised learning for cell-level visual representation in histopathology images with generative adversarial networks," *IEEE J. Biomed. Health Inform.*, vol. 23, no. 3, pp. 1316-1328, 2018.
- [32] K. Stacke, C. Lundström, and G. Eilertsen, "Evaluation of contrastive predictive coding for histopathology applications," in *Proceedings of the Machine Learning for Health, NeurIPS Workshop*, 2020, pp. 328-340.
- [33] O. Ciga, T. Xu, and A. L. Martel, "Self supervised contrastive learning for digital histopathology," *Mach. Learn. Appl.*, vol. 7, p. 100198, 2022.
- [34] N. A. Koohbanani, B. Unnikrishnan, S. A. Khurram, P. Krishnaswamy, and N. Rajpoot, "Self-path: Self-supervision for classification of pathology images with limited annotations," *IEEE Trans. Med. Imaging*, vol. 40, no. 10, pp. 2845-2856, 2021.
- [35] B. McMahan, E. Moore, D. Ramage, S. Hampson, and B. A. y Arcas, "Communication-efficient learning of deep networks from decentralized data," in *Proceedings of the 20th International Conference on Artificial Intelligence and Statistics*, 2017, vol. 54, pp. 1273-1282.
- [36] T. Li, A. K. Sahu, M. Zaheer, M. Sanjabi, A. Talwalkar, and V. Smith, "Federated optimization in heterogeneous networks," in *Proceedings of Machine Learning and Systems (MLSys)*, vol. 2, pp. 429-450, 2020.
- [37] S. P. Karimireddy, S. Kale, M. Mohri, S. Reddi, S. Stich, and A. T. Suresh, "SCAFFOLD: Stochastic controlled averaging for federated learning," in *Proc. Int. Conf. Mach. Learn. (ICML)*, 2020, pp. 5132-5143.
- [38] J. Wang, Q. Liu, H. Liang, and G. Joshi, "Tackling the objective inconsistency problem in heterogeneous federated optimization," in *Proc. Adv. Neural Inf. Process. Syst. (NeurIPS)*, 2020, vol. 33, pp. 7611-7623.
- [39] H. Wang, M. Yurochkin, Y. Sun, D. Papailiopoulos, and Y. Khazaeni, "Federated learning with matched averaging," in *International Conference on Learning Representations (ICLR)*, 2020.
- [40] T.-M. H. Hsu, H. Qi, and M. Brown, "Measuring the effects of non-identical data distribution for federated visual classification," *arXiv preprint, arXiv: 1909.06335*, 2019.
- [41] Y. Xia, D. Yang, W. Li, A. Myronenko, D. Xu, H. Obinata, *et al.*, "Auto-FedAvg: Learnable federated averaging for multi-institutional medical image segmentation," *arXiv preprint, arXiv: 2104.10195*, 2021.
- [42] M. Andreux, J. O. du Terrail, C. Beguier, and E. W. Tramel, "Siloe federated learning for multi-centric histopathology datasets," in *Domain Adaptation and Representation Transfer, and Distributed and Collaborative Learning*, Cham, 2020, pp. 129-139.
- [43] A. Karnewar and O. Wang, "Multi-scale gradients for generative adversarial networks," in *Proceedings of the IEEE/CVF Conference on Computer Vision and Pattern Recognition (CVPR)*, 2020, pp. 7799-7808.
- [44] Y. Zhang and Q. Yang, "A survey on multi-task learning" *IEEE Trans. Knowl. Data Eng.*, pp. 1-20, 2021.
- [45] K. He, X. Zhang, S. Ren, and J. Sun, "Deep residual learning for image recognition," in *Proceedings of the IEEE/CVF Conference on Computer Vision and Pattern Recognition (CVPR)*, 2016, pp. 770-778.
- [46] T. Araújo, G. Aresta, E. Castro, J. Rouco, P. Aguiar, C. Eloy, A. Polónia, *et al.*, "Classification of breast cancer histology images using convolutional Neural Networks," *PLoS One*, vol. 12, no. 6, p. e0177544, 2017.
- [47] I. Fondón, A. Sarmiento, A. I. García, M. Silvestre, C. Eloy, A. Polónia, *et al.*, "Automatic classification of tissue malignancy for breast carcinoma diagnosis," *Comput. Biol. Med.*, vol. 96, pp. 41-51, 2018.
- [48] G. Aresta, T. Araújo, S. Kwok, S. S. Chennamsetty, M. Safwan, V. Alex, *et al.*, "BACH: Grand challenge on breast cancer histology images," *Med. Image Anal.*, vol. 56, pp. 122-139, 2019.
- [49] X. Li, M. Jiang, X. Zhang, M. Kamp, and Q. Dou, "FedBN: Federated learning on non-iid features via local batch normalization," in *International Conference on Learning Representations (ICLR)*, 2021.
- [50] M. Adnan, S. Kalra, J. C. Cresswell, G. W. Taylor, and H. R. Tizhoosh, "Federated learning and differential privacy for medical image analysis," *Sci. Rep.*, vol. 12, no. 1, p. 1953, 2022.